Spatial Ring Current Model for the Prismane Molecule

Stefano Pelloni* and Paolo Lazzeretti

Dipartimento di Chimica, Università degli Studi di Modena e Reggio Emilia, Via Campi 183, 41100 Modena, Italy

Received: December 21, 2007; Revised Manuscript Received: March 5, 2008

Spatial models of magnetic-field induced electronic ring currents have been constructed for the prismane molecule via stagnation graphs and current density maps. These tools provide an insight into the complicated phenomenology resulting from competition of diatropic and paratropic regimes that determine the magnitude of various components of magnetic susceptibility and magnetic shielding of hydrogen and carbon nuclei. Shielding density maps show that the differential Biot−Savart law, along with an atlas of the current density field, explains magnetic shielding at hydrogen and carbon nuclei and virtual shielding at ring and cage centers.

1. Introduction

Prismane is a polycyclic hydrocarbon with chemical formula C_6H_6. Its systematic name is tetracyclo[2.2.0.0.^{2,6}.0^{3,5}]hexane.[1,2] The six carbon atoms of the prismane molecule are arranged in the shape of a right prism, in which the top and bottom triangular faces, connected by a ribbon of three rectangles, lie on top of each other. Albert Ladenburg suggested this structure for the far more stable isomer compound now known as benzene,[3] but the theory that benzene is a prismatic molecule turned out to be wrong, as shown shortly afterward by Kekulè.[4]

Appealing features of prismane were theorized upon,[5–8] but the molecule continued to exist only in theory, until it was first synthesized[2] in 1973, 104 years after Ladenburg's speculation.[3]

The special properties of this compound arise from high strain of its cage structure, which makes synthesis of the molecule difficult. It is a colorless liquid, stable at room temperature, but it is explosive.[2] As for cyclopropane, the shrinking of the C−C−C bond angles, from 109.47° in a tetrahedron to 60° in an equilateral triangle, causes high tension. Four carbon atoms lie on the same plane, in a rectangular configuration which is not that of equilibrium for cyclobutane. Consequently, the bonds have a low bond energy and break at a low activation energy. On the other hand, the hexamethylprismane molecule, in which the six hydrogens are replaced by CH_3- groups, is more stable and it can be synthesized by rearrangement reactions.[1]

Recent computational studies examined the energetic stability of prismane in relation to other benzene isomers.[9,10] Relative bond strengths in tetrahedrane, prismane, and some of their aza analogues were evaluated.[11] Ab initio analysis of C−H and C−C stretching intensities in Raman spectra of prismane was reported.[12]

The competition between σ-aromatic and antiaromatic behavior resulting from the simultaneous presence of three- and four-membered carbon rings in the same cage, has been discussed.[13] Unusual magnetic properties are expected from the conflict of diatropic and paratropic response of the electron distribution for a prismane molecule in the presence of magnetic fields perpendicular to either triangular or rectangular faces.

An assessment of magnetic response of prismane constitutes the aim of the present paper, which is organized as follows. Theoretical methods and computational tools used to build up a model visualizing the electron flow in the presence of magnetic field are described in section 2. The actual model consists of stagnation graphs and maps of current density. It is presented in section 4, in which its ability to rationalize near Hartree−Fock predictions of magnetic susceptibility and magnetic shielding of hydrogen and carbon nuclei is demonstrated. Shielding density maps examined in section 5 provide auxiliary instruments for understanding magnetotropicity of prismane.

2. Models of the Current Density Field via Stagnation Graphs

The linear response to an external magnetic field $\mathbf{B}$ of a diamagnetic molecule, that is, a system even under time reversal, is determined by the induced electronic current density $\mathbf{J}^{\mathbf{B}}$, a continuous vector function in 3-dimensional space. It is divergenceless for a stationary flow, and its modulus $|\mathbf{J}^{\mathbf{B}}|$ is proportional to the applied field. Quantum mechanical methods are currently used to evaluate $\mathbf{J}^{\mathbf{B}}(\mathbf{r})$ allowing for approximate computational schemes. Second-rank tensor properties, for example, magnetizability $\chi_{\alpha\beta}$ and magnetic shielding $\sigma^{I}_{\alpha\beta}$ at nucleus I, with position $\boldsymbol{R}_I$, can efficiently be evaluated in terms of the magnetically induced current density via relationships of classical electromagnetism.[14]

A set of reasons justifying this theoretical approach to molecular magnetic response is provided by the Hirschfelder concept of *subobservable*.[15] The charge density $\rho(\mathbf{r})$ and the current density $\mathbf{J}(\mathbf{r})$ are expectation values of corresponding quantum mechanical operators. If these expectation values are given as functions of position in the real space, the properties of interest can be evaluated with no explicit reference to the molecular wave function. Theoretical procedures for doing the job have been developed by McWeeny.[16–18]

The formalism based on $\rho(\mathbf{r})$ and $\mathbf{J}(\mathbf{r})$ is characterized by a number of nice advantages: (i) practicality and economy of thinking obtained by the use of functions in $\mathbb{R}^3$, instead of wave functions that depend on $3n$ space-spin coordinates for an n-electron molecule, (ii) visualization of interaction paths via graphic models showing streamlines and modulus of the current density vector field, (iii) quantitative estimate of contributions to the response properties from different molecular domains, and (iv) rationalization of the response mechanism in simple

* Corresponding author. E-mail: pelloni.stefano@unimo.it.

10.1021/jp711996n CCC: $40.75
Published on Web 05/14/2008

TABLE 1: Magnetizability[a] of Prismane in 10^{29} JT^{-2}

$\chi_{\parallel}^{d}$	$\chi_{\perp}^{d}$	$\Delta\chi^{d}$	$\chi_{\parallel}^{p}$	$\chi_{\perp}^{p}$	$\Delta\chi^{p}$	$\chi_{\parallel}$	$\chi_{\perp}$	$\bar{\chi}$	$\Delta\chi$
−412.2	−501.4	89.2	266.8	435.7	−168.9	−145.4	−65.7	−92.2	−79.7

[a] Diamagnetic and paramagnetic contributions from the CO approach (origin in the center of mass). Nearly identical results obtained via the CTOCD-DZ and DZ2 approaches are given as Supporting Information. The || and ⊥ symbols denote zz and $xx = yy$ components, respectively, and $\Delta\chi = \chi_{\parallel} - \chi_{\perp}$.

TABLE 2: Magnetic Shielding Tensors and Chemical Shift of C and H in Prismane[a]

	xx	yy	zz	av
σ^{C}	135.6	140.0	229.1	168.2
δ^{C}				26.5
δ^{C} exptl [b]				30.6
σ^{H}	29.32	26.29	34.59	30.07
δ^{H}				2.11
δ^{H} exptl [c]				2.28

[a] Values in ppm, calculated via the damped CTOCD-DZ2 method.[35] The ^{13}C and ^{1}H tensors are given in the coordinate system specified in the text: the origin is in the center of mass (CM), the z axis coincides with the C_3 symmetry axis and the x axis is orthogonal to a rectangular face. Coordinates used in the calculations, in bohr: C (1.6420773978, 0.0, 1.4620961152), H (3.1328463254, 0.0, 2.8284889474). All shifts from tetramethylsilane. Absolute TMS values calculated via the CTOCD-DZ2-CHF procedure[27] with the same C and H basis set used here, and an uncontracted (13s10p3d2f) aug-cc-pVTZ basis set[36] for Si are $\sigma_{av}^{H} = 32.18$ for ^{1}H and $\sigma_{av}^{C} = 194.7$ ppm for ^{13}C. [b] In C_6D_6, from Katz and Acton.[2] [c] In CCl_4, from Katz and Acton.[2]

TABLE 3: Virtual Shielding in ppm at Various Distances (in bohr) along the x and z Axes

point	xx	yy	zz	av
CM[a]	− 25.6	− 25.6	55.2	1.3
Triangular Face				
$z = 1.4621$[b]	32.1	32.1	46.8	37.0
$z = 2.8285$[c]	7.8	7.8	38.7	18.1
$z = 3.5$	0.6	0.6	30.3	10.5
$z = 4.5$	− 1.4	− 1.4	19.2	5.4
Rectangular Face				
$x = -0.8210$[b]	− 59.5	8.7	57.1	2.1
$x = -1.5664$[c]	− 54.6	4.4	41.0	− 3.1
$x = -2.5$	− 20.3	− 6.2	9.7	− 5.6
$x = -3.5$	− 1.7	− 5.4	− 3.1	− 3.4

[a] Origin in the center of mass. [b] Plane of carbon nuclei. [c] Plane of hydrogen nuclei. Values in ppm, calculated via the damped CTOCD-DZ2 method.[35]

terms, allowing for classical tools such as the Ampère and the Biot−Savart laws.[19]

These relationships can be written in concise form employing tensor notation. Allowing for the Einstein implicit summation rule over repeated suffixes, using the Levi−Civita third-rank unit pseudotensor $\epsilon_{\alpha\beta\gamma}$, and introducing a current density tensor via the derivative[20]

$$\mathscr{J}_{\alpha}^{B_\beta}(\mathbf{r}) = \frac{\partial}{\partial B_\beta} J_{\alpha}^{B}(\mathbf{r}), \tag{1}$$

the magnetic susceptibility and the magnetic shielding at nucleus I are defined via the equations[21]

$$\chi_{\alpha\delta} = \frac{1}{2}\epsilon_{\alpha\beta\gamma}\int r_\beta \mathscr{J}_{\gamma}^{B_\delta}(\mathbf{r}) d^3r \tag{2}$$

$$\sigma_{\alpha\delta}(\mathbf{R}_I) \equiv \sigma_{\alpha\delta}^{\mathrm{I}} = -\frac{\mu_0}{4\pi}\epsilon_{\alpha\beta\gamma}\int \frac{r_\beta - R_{I\beta}}{|\mathbf{r} - \mathbf{R}_I|^3}\mathscr{J}_{\gamma}^{B_\delta}(\mathbf{r})\, \mathrm{d}^3r \tag{3}$$

Multiplying both sides of relationship 3 by B_δ one obtains the integral Biot−Savart (IBS) law[19] for the magnetic flux density

$$B_{ind,\alpha}(\mathbf{R}_I) = -\sigma_{\alpha\delta}^{\mathrm{I}} B_\delta \tag{4}$$

induced at $\mathbf{R}_I$. The integrand in eq 3 is a shielding density tensor function[22,23] in $\mathbb{R}^3$. Therefore, the element of magnetic field induced in the α direction on a nuclear probe at $\mathbf{R}_I$ by the current density generated at point $\mathbf{r}$ by an external magnetic field applied in the δ direction, is

$$\mathrm{d}B_{ind,\alpha}(\boldsymbol{R}_I) = -\Sigma_{\alpha\delta}^{\mathrm{I}}(\mathbf{r}) B_\delta\, \mathrm{d}^3r \tag{5}$$

The zz component of the shielding density is

$$\Sigma_{zz}^{\mathrm{I}}(\mathbf{r}) = -\frac{\mu_0}{4\pi}\epsilon_{z\beta\gamma}\frac{r_\beta - R_{I\beta}}{|\mathbf{r} - \mathbf{R}_I|^3}\mathscr{J}_{\gamma}^{B_z}(\mathbf{r}) \tag{6}$$

The current density determines the properties, eqs 2 and 3, of a system in a magnetic field. Therefore, a careful study of the $\mathbf{J}^{\mathbf{B}}$ vector function yields detailed information on the mechanism of molecular response.

The topology of the field deserves special attention. Critical points, where the modulus $|\mathbf{J}^{\mathbf{B}}|$ vanishes, correspond to various forms of the Jacobian matrix $\nabla_\alpha J_\beta^{\mathbf{B}}$. They are identified by typical phase portraits which are algebraically distinct from one another.[21] Shape and structure of the current density field are determined by locating these points in the real space and by assembling them in a graph, which provides the essentials for an understanding of molecular magnetism in visual terms.

In the tail regions of a diatropic molecule in the presence of magnetic perturbation, the electron cloud rotates counterclockwise about an axis that coincides with the direction of $\mathbf{B}$. Since the electron charge is negative, the current density $\mathbf{J}^{\mathbf{B}}$ rotates the other way round, that is, clockwise. The local regime is Larmor-type, that is, vortical diamagnetic: maps at right angles to $\mathbf{B}$ show closed streamlines with the shape of topological circumferences, customarily termed "ring currents".

In the outer domains of the molecule, $|\mathbf{J}^{\mathbf{B}}|$ vanishes along a central line that is a continuous path of vortical stagnation points (SP), normal to the circular diamagnetic current flow. It is termed *primary* vortical stagnation line (SL) of the n-electron "fluid".

The structure of the $\mathbf{J}^{\mathbf{B}}$ vector field becomes more complicated on approaching molecular regions of higher $\rho(\mathbf{r})$, for example, close to the nuclear framework, where transition between different regimes usually occurs. The current density field in the vicinity of the nuclei is characterized by typical patterns, for example, saddles and vortices that can be either diamagnetic or paramagnetic.[24] Their phase portraits are observed in streamline maps.[21] Continuous paths of saddle points may form saddle SLs.[25]

Nonisolated SPs lying on stagnation paths, along with the isolated critical points, fully characterize the current distribution. The set of isolated SPs and stagnation paths has been called a stagnation graph (SG) by Gomes.[25] An SG contains fundamental information on the salient features of the $\mathbf{J}^{\mathbf{B}}(\mathbf{r})$ vector field. It provides a portable spatial model of current flow in abridged

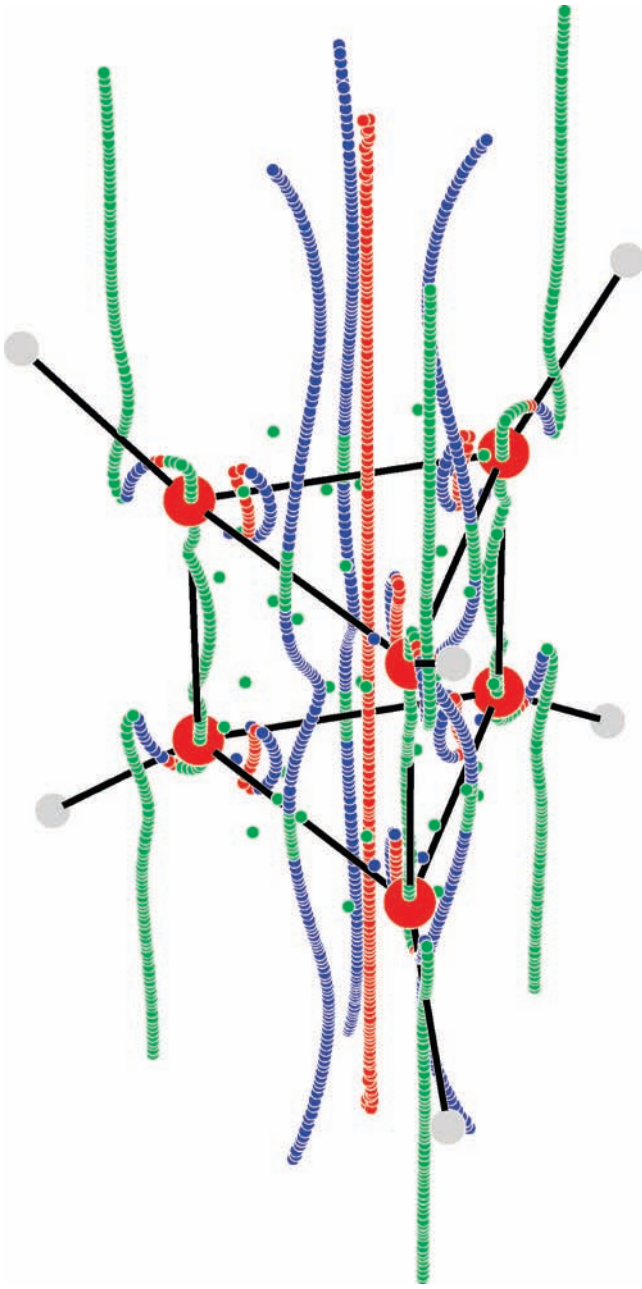

Figure 1. Perspective view of the stagnation graph of the current density vector field in prismane C_6H_6. The uniform external magnetic field $\mathbf{B} = \epsilon_3 B_z$ is perpendicular to the triangular faces (ϵ_3 is the unit vector in the direction of the z axis through the center). Green (red) points denote diamagnetic (paramagnetic) vortices; saddle points are blue.

and compact form, showing domains of diatropic and paratropic currents. Therefore, an SG indicates how to build up an atlas consisting of a minimum number of current density maps, indispensable for an overall description and for an assessment of magnetotropicity of molecules. Previous investigations demonstrated the practicality of SGs for understanding magnetic response of conjugated cyclic molecules,[26] cyclopropane,[27] [2.2]para-cyclophane,[28] and heterocyclic pentatomics.[29,30]

3. Details of Calculation

A (13s10p5d2f/8s4p1d) uncontracted Gaussian basis set, used for an assessment of diatropicity of cyclopropane,[27,31,32] was employed to optimize the molecular geometry of prismane at the Hartree−Fock level of theory by the Gaussian 98 code[33] and to calculate the magnetic properties via the coupled Hartree−Fock (CHF) approach implemented in the SYSMO package.[34] The numerical DZ2 and PZ2 variants[35] of a procedure based on continuous transformation of the origin of the current density-diamagnetic zero (CTOCD-DZ) and paramagnetic zero (CTOCD-PZ) were applied.[21] Calculated values of magnetic susceptibilities and magnetic shieldings of ^{1}H, ^{13}C nuclei and of virtual probes at cage and ring centers are shown in Tables 1, 2, and 3. (The predictions from different approximations are virtually identical in most cases, indicating that near Hartree−Fock accuracy has been attained. Therefore only the DZ2 nuclear magnetic shieldings were reported.) Rationalization of magnitude and sign of nuclear shielding tensors is discussed in section 5.

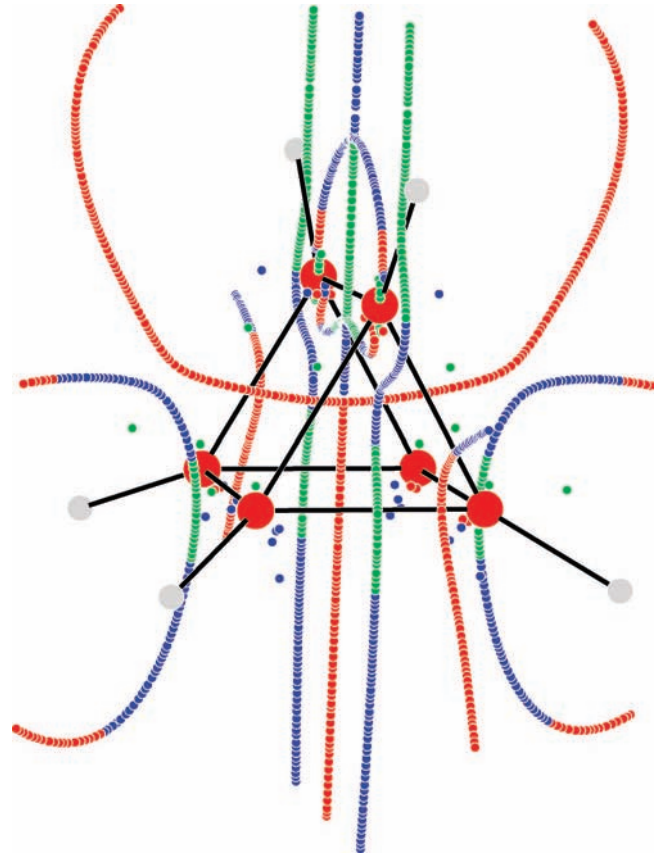

Figure 2. Perspective view of the stagnation graph of the current density vector field in prismane C_6H_6. The uniform external magnetic field $\mathbf{B} = \epsilon_1 B_x$ is perpendicular to a rectangular face (ϵ_1 is the unit vector in the direction of the x axis through the center). The color code is the same as in Figure 1.

4. Ring Current Model of Prismane

Let us consider a coordinate system with origin in the center of mass (CM) of prismane. The $x(z)$ direction is assumed perpendicular to a rectangular (triangular) prism face. A perspective view of the SG of the prismane molecule in a magnetic field $\mathbf{B}\|\epsilon_3$, at right angles to the triangular faces, is shown in Figure 1. It looks like two superimposed SGs of cyclopropane.[27]

An SG is usually a complicated topological object hard to represent in two dimensions. A graphic software, delivered as supporting material available (SMA), can be used to observe the features of the SG in detail, by rotating and blowing it up.[37]

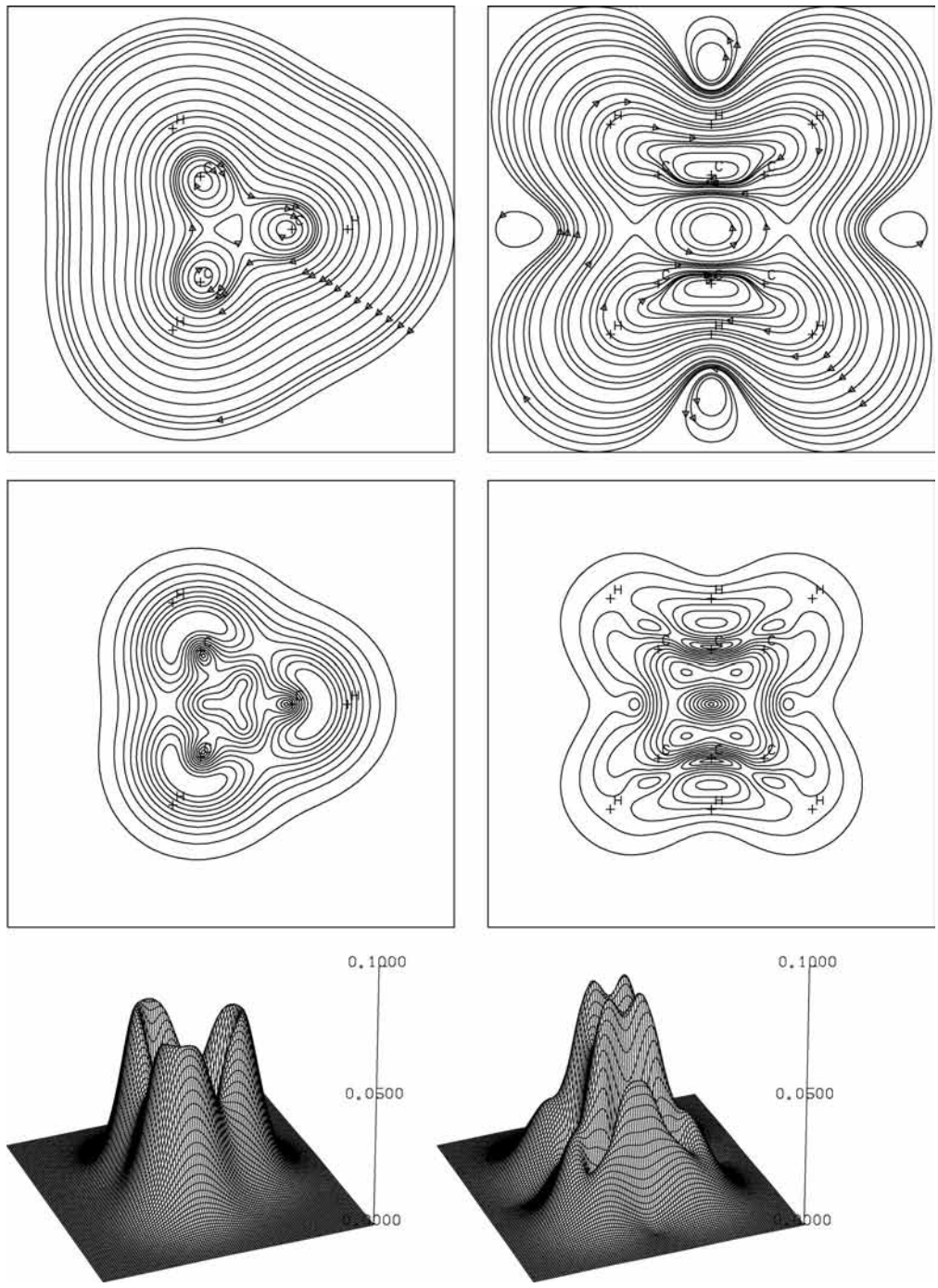

Figure 3. Streamlines and modulus of the current density vector field induced in prismane by a magnetic field with magnitude of 1 au. On the left (right), the applied B_z (B_x) is normal to a triangular (rectangular) face and directed outward. The plot planes pass through the center of mass at the origin. The projection of atom positions is marked by a cross. The maximum modulus (step between two consecutive contours) in au is 0.066 (0.006) on the left, and 0.078 (0.007) on the right. The maximum value of the benzene π-ring current computed at the same level of theory is 0.08 au in the 1 a_0 plane.

This software is useful for a better understanding of the following discussion.

The primary diamagnetic vortical SL, coinciding with the $C_3 \equiv z$ symmetry axis, unfolds into four vortical and three saddle SLs at two points, equally spaced from CM, which lie at a distance $|z_0| > 10$ bohr from it. They are termed branching points (BP) of the SG. This splitting is regulated by an index conservation theorem discussed by Gomes.[25,38] The index characterizing a stagnation point counts the number of times $\mathbf{J^B}$ rotates completely while one walks counterclockwise around a circle of radius ϵ, so small that $\mathbf{J^B}$ has no zeroes inside except the SP at its center. The topological index ι of a saddle (vortex) line is -1 $(+1)$.[39,40] When a stagnation line of index ι_0 splits into m new lines, the sum of the indices of the m stagnation lines emerging from the branching point is

$$\sum_{k=1}^{m} \iota_k = \iota_0. \tag{7}$$

The portions of primary SL lying beyond the outermost BPs are not shown in Figure 1. They correspond to diamagnetic circulation in the far-out regions of the molecule.

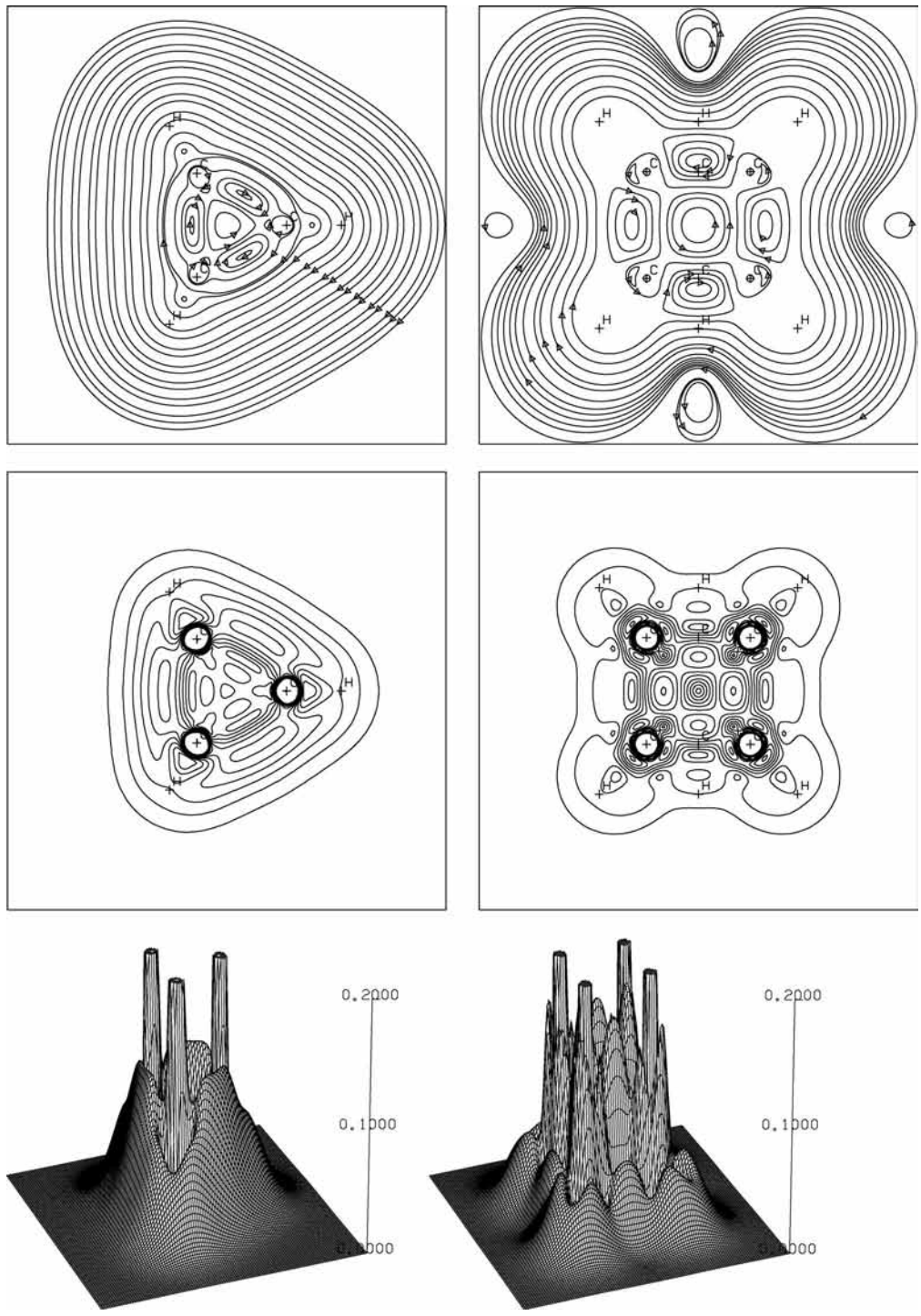

Figure 4. Streamlines and modulus of the current density vector field induced in prismane by a magnetic field with magnitude 1 au. The atom positions are marked by a cross (the graphical conventions are the same as in Figure 3). On the left (right), the triangular (rectangular) face lies on the plot plane at $z = 1.4621$ ($x = -0.8210$) bohr. The maximum modulus (step between two consecutive contours) in au 0.605 (0.02) on the left, 1.760 (0.02) on the right. Values higher than 0.2 were cut. A magnified representation of flow in the proximity of the C nuclei (white region in the top-right map, is given as SMA.

Three vortical SLs, with green color in Figure 1, originate and terminate at the two BPs, and extend in-between for $|z| \approx 10$ bohr in the direction of **B**. They pass through the center of small-radius diamagnetic whirlpools, visible in streamline maps on planes normal to the z axis, for example, Figure 3. These SLs lie on the σ_v symmetry planes, alongside the C−C bonds of the rectangular faces. After going across the carbon nuclei, they bend outward, approximately in the direction of the carbon sp^3 hybrid orbitals forming C−H bonds. The fourth vortical SL, with red color, corresponds to the central paramagnetic vortex typical of ring structures.[21] It contains a path of SPs with $|z| \leq z_0$.

The four basins of vortical flow are enclosed in topologycal cylinders, shrinking and joining in a neighborhood of the outermost BPs. (These surfaces have the shape of bean pods that share common ribs). They are separated by three saddle SLs (the ribs), represented in blue in Figure 1, which lie on the σ_v symmetry planes. They bend toward the C_3 axis and traverse the rectangular faces in two points. On crossing the plane of the triangular faces, the saddle regime becomes vortical

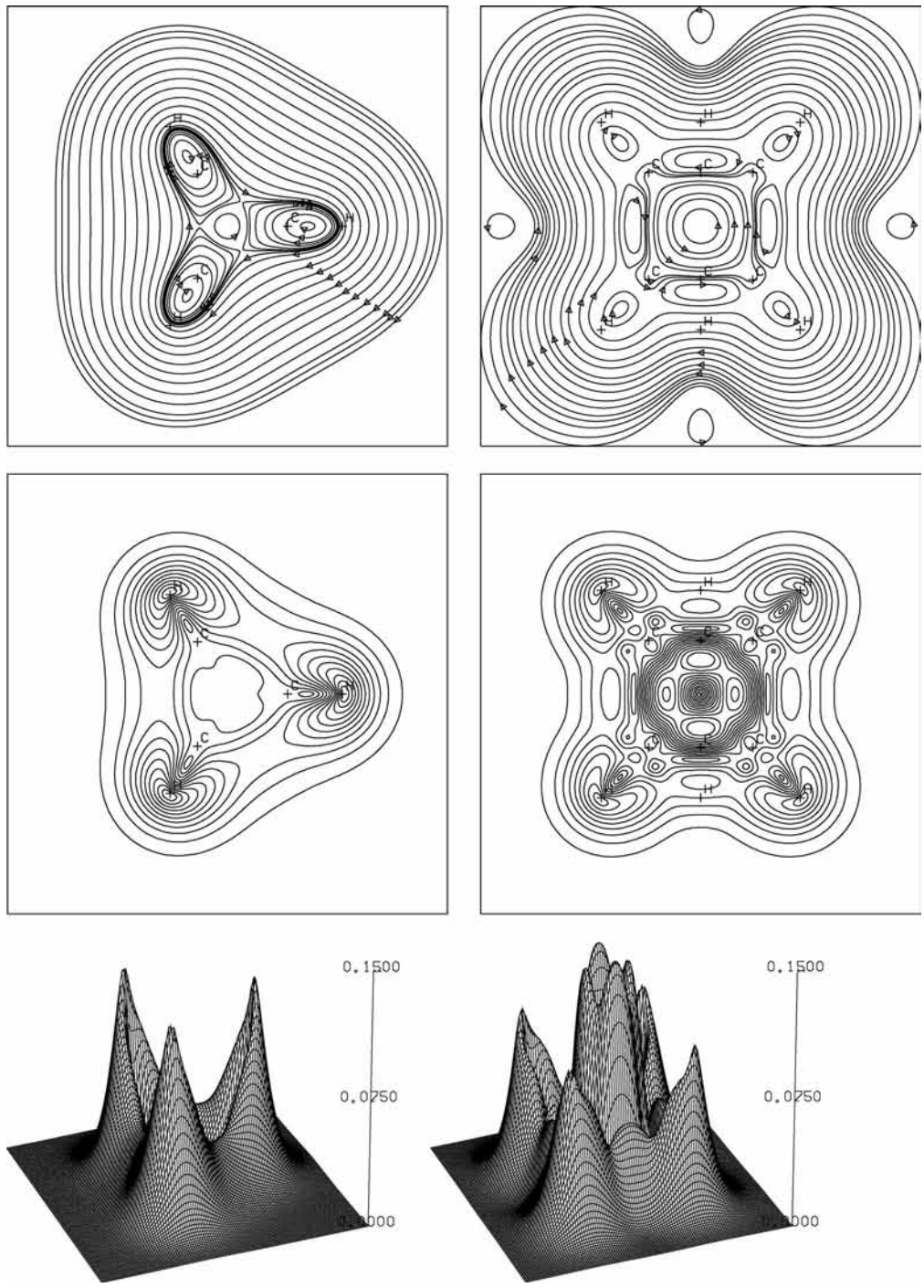

Figure 5. Streamlines and modulus of the current density vector field induced in prismane by a magnetic field of magnitude 1 au. The graphical conventions are the same as in Figure 3. On the left (right), three (four) equivalent H nuclei lie on the plot plane at $z = 2.8285$ ($x = -1.5664$) bohr. The maximum modulus (step between two consecutive contours) in au 0.118 (0.01) on the left, 0.140 (0.01) on the right.

diamagnetic in a small region around the short green portion of SL slightly outside of the midpoint of the C−C bonds. In the cyclopropane molecule this green line shrinks to a point.[27] Closed disconnected stagnation loops, containing vortical and saddle portions of SL, are observed near-by the C nuclei.

The pattern of stagnation lines in Figure 1 is consistent with the streamline maps on the top-left corner of Figures 3–5, obtained by Runge−Kutta integration of the system of differential equations for the flow[21] in three plot planes, at various distances on the C_3 axis, namely, the $z = 0$, $z = 1.4621$ (the C triangle), and $z = 2.8285$ bohr (the three proton plane). They denote local diatropic regime about the edges of the lateral surface, paratropic flow about the central red line, and saddle-flow about the blue lines separating vortices. The overall features are analogous to those previously observed for cyclopropane.[27]

The SG in Figure 1 provides a fundamental link among the maps of Figures 3,4, and 5, showing how they are related to one another in the space. It is useful to understand how the features of the current density field continuously change moving along the vertical direction, in connection with splitting of stagnation paths.

The SG of the prismane molecule in a magnetic field **B** directed as the x axis normal to one rectangular face is shown

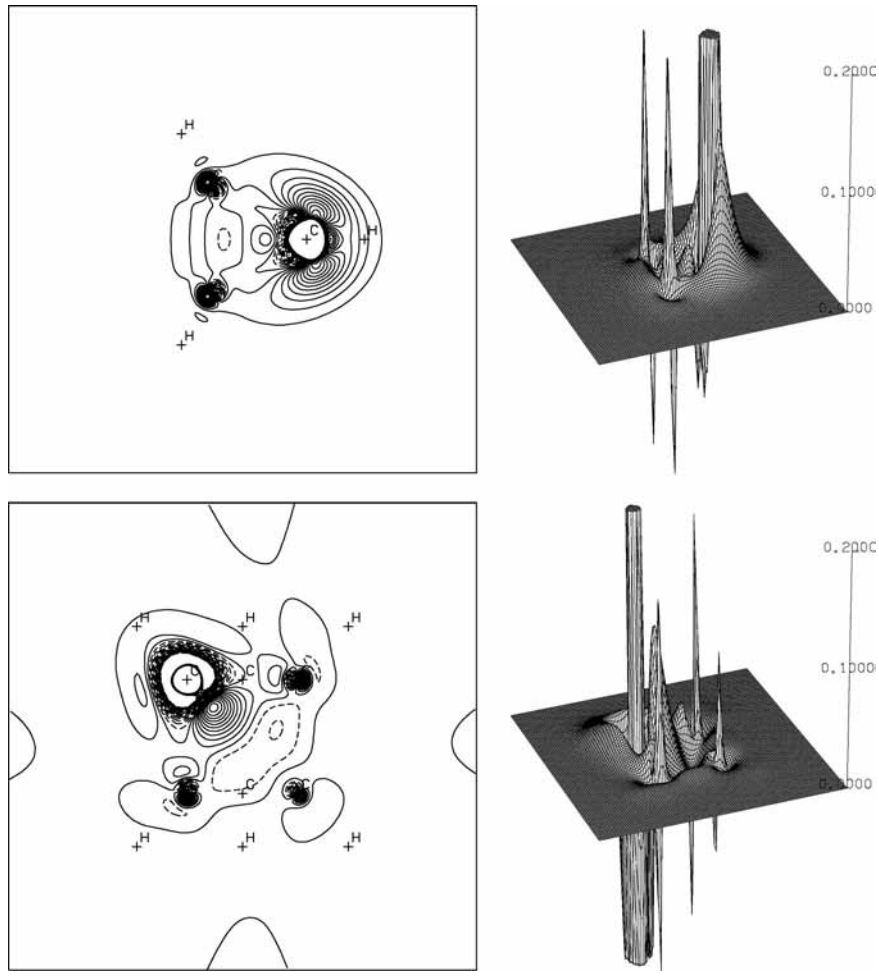

Figure 6. Magnetic shielding densities Σ^{C}_{zz} on the plane of the C nuclei of the triangular face (above) and Σ^{C}_{xx} on the plane of the rectangular face (below) of prismane, in au. Truncated values of minimum ÷ maximum ÷ step: −0.20 ÷ 0.20 ÷ 0.01. The contributions to the probe C nucleus from a spike-up and spike-down pair on remote carbon atoms nearly cancel out.

in Figure 2. The central red SL crossing the plane of four carbon atoms indicates local paratropic regime. At a BP in the proximity of CM, this SL splits up, giving rise to a couple of red lines, which diverge going across the other rectangular faces, and to a short segment of blue saddle SL. Slightly below a C−C bond, another BP of the central SL is observed, at which three green diatropic vortical SLs start. Further splitting occurs above the midpoint of the C−C bond, where the central green SL branches out into three blue saddle lines. These splittings are consistent with the Gomes theorem.[25,38]

The SG contains short segments of green SL in the external parts, facing the sides of the carbon rectangle. Each SP within these segments corresponds to a diatropic whirlpool that flows in a plane normal to the direction of the local tangent to the SL. These diamagnetic vortices are sustained by the electron charge outside of the C−C bonds. Blue lines denote local saddle-flow in the regions beyond the ends of these green segments.

The two continuous stagnation paths, in front of the longer C−C bond of the rectangular face, contain blue (green) lines, which extend to the tail regions, in the negative (positive) x direction, and mark regions of saddle (vortical diatropic) circulation. The SG of Figure 2 was efficiently used to obtain a minimal set of current density maps that constitute the model of electron flow for prismane in a field normal to a rectangular face. Without its help, it would be hard to understand the connections among the streamline maps shown on the top-right corner of Figures 3–5 for three plot planes at various distances from CM.

The general features of the $\mathbf{J}^{\mathbf{B}}$ field in the peripheral regions are not dramatically different from those observed for **B** normal to the triangular face, for example, diatropic flow takes place in a wide domain around the protons, and diamagnetic vortices are found about the C−C bonds of the rectangular face. Maximum intensity is attained in the vicinity of the carbon nuclei, as shown in the contour maps and in the three-dimensional perspective view for the modulus $|\mathbf{J}^{\mathbf{B}}|$ in Figures 3–5.

The intensity of the central paratropic whirlpool normal to the triangular face is fairly negligible. On the contrary, the paratropic regime about the central (red) vortical line, coincident with the x axis, stands in sharp contrast to that characterizing the currents about the z direction. The intensity of the paramagnetic vortex is much stronger, and its radius is from two to three times larger. At the edge of the paramagnetic stream about the C_2 axis perpendicular to the rectangular face, the calculated modulus $|\mathbf{J}^{\mathbf{B}}|$ reaches local maximum values ≈ 0.08, 0.18, and 0.13 au, respectively at $x = 0$, −0.8210, and −1.5664 bohr, that is, CM, carbon, and hydrogen planes.

These measures account for strong paratropicity. (They can be compared with the corresponding quantity for the π ring current in benzene. Using the same CTOCD-DZ2 level of theory and the same basis set, maximum $|\mathbf{J}^{\mathbf{B}}|$ for benzene is 0.08 au on a plane at 1 bohr above that of the molecule.[21]) Two representations magnified for closer inspection are given in the SMA. The portraits of two foci[21] are visible near-by each carbon nucleus.

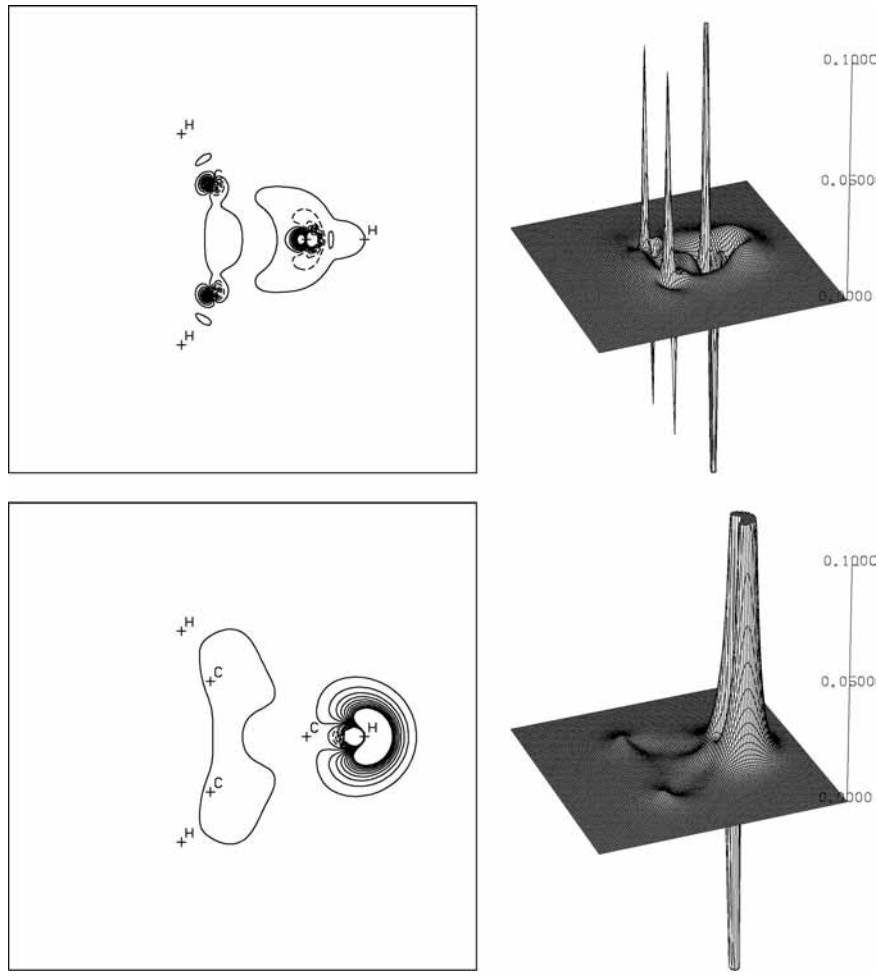

Figure 7. Magnetic shielding density Σ^{H}_{zz} on two parallel planes, containing the C nuclei of the triangular face, at $z = 1.4621$ bohr (above), and three H nuclei, at $z = 2.8285$ bohr (below), in au. Truncated values of minimum ÷ maximum ÷ step: −0.10 ÷ 0.10 ÷ 0.01.

5. Shielding Density Maps

The usefulness of the map $\mathbf{J^B}(\mathbf{r}) \rightarrow \Sigma^{I}(\mathbf{r})$, see eq 6, for the interpretation of magnetic shielding cannot be overemphasized. Plots of the density functions[22,23] $\Sigma^{I}_{zz}(\mathbf{r})$ and $\Sigma^{I}_{xx}(\mathbf{r})$, given in Figures 6–9 for I ≡ C, H, and CM, weigh the dual role of various molecular domains, by discriminating their shielding or deshielding contributions at a probe.

The effect of a current circuit is explained via rules outlined in detail elsewhere.[27,32,41,42] Allowing for eqs 1, 5, and 6, the sign of the element of magnetic field $d\mathbf{B}_{ind}(\mathbf{R}_I)$, induced on a probe at $\mathbf{R}_I$ by the current density $\mathbf{J^B}(\mathbf{r})$, is determined by the sine of the angle θ (positive for an anticlockwise rotation) between the vectors $\mathbf{J^B}(\mathbf{r})$ and $\mathbf{R}_I - \mathbf{r}$. For $0 < \theta < \pi$ ($\pi < \theta < 2\pi$), the element of flux density is positive (negative). According to eqs 5 and 6, one can alternatively state that the current density $\mathbf{J^B}(\mathbf{r})$, induced by an external magnetic field B_z, deshields (shields) the probe by providing a negative (positive) $\Sigma^{I}_{zz}(\mathbf{r})$ value to the integral (3) for total σ^{I}_{zz}. Contributions with opposite signs to shielding density at a probe site arise from the opposite senses of flow of closest and furthest portions of a distant current loop. By superimposing corresponding contour shielding densities, Figures 6–9, and streamlines, Figures 3–5, it is easy to verify that shielding (deshielding) regions match neighborhoods of negative (positive) values of sin θ.

Theoretical values of shielding components are promptly rationalized in this way via shielding density plots. Hereafter we discuss a few relevant results for C, H, and CM in prismane.

Let the applied field B_z (B_x) be perpendicular to a triangular (rectangular) face, then the shielding component of interest is σ^{I}_{zz} (σ^{I}_{xx}), with associated shielding density Σ^{I}_{zz} (Σ^{I}_{xx}). The maps of Figures 3–9 show that, according to the rule quoted above, the near-by (remote) portion of a diamagnetic current circuit creates a field that reinforces (diminishes) the external field at, and hence has a deshielding (shielding) effect on, the probe. The opposite effect is produced by a paramagnetic loop.

The strong anisotropy $\Delta\sigma^{C} = \sigma^{C}_{zz} - (\sigma^{C}_{xx} + \sigma^{C}_{yy})/2 = 91.3$ ppm of carbon shielding in Table 2 is explained by the maps in Figure 6. Intense deshielding taking place in an annular region around a C nucleus lowers the value of σ^{C}_{xx}, as shown by contour and three-dimensional plots in the bottom of the figure. On the other hand, the strong upfield value of σ^{C}_{zz} is due to a small-radius diamagnetic vortex sustained by a 1s inner shell and sp^3 hybrid orbitals forming C−H and C−C bonds. It flows about each C nucleus and winds to a large extent in the z direction above and below a triangular face, see the SG of Figure 1 and modulus maps in Figures 3–5. This pattern is similar to that observed for cyclopropane.[27]

An analogous diamagnetic shift increases the component $\sigma^{H}_{zz} \approx 34.6$ ppm and enhances the anisotropy $\Delta = \sigma^{H}_{zz} - (\sigma^{H}_{xx} + \sigma^{H}_{yy})/2 \approx 7$ ppm of proton shielding. The σ^{H}_{zz} component evaluated in cyclopropane via the same basis set[27] is bigger, ≈37.0 ppm. This can be explained by observing that, in C_3H_6, the proton lies inside the diamagnetic vortex flowing near-by a C−H bond, cf., the bottom-left map in Figure 2 of ref 27, therefore it is

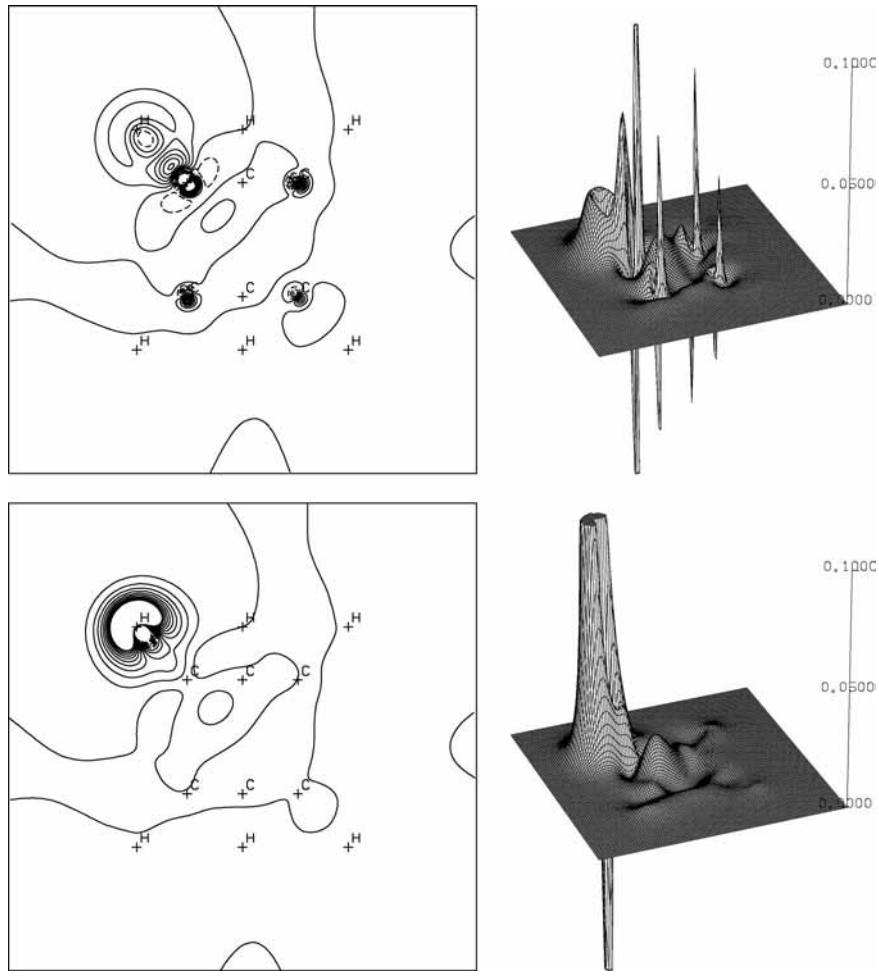

Figure 8. Magnetic shielding density Σ_{xx}^{H} on two parallel planes, containing the C nuclei of the rectangular face at $x = -0.8210$ bohr (above), and four H nuclei at $x = -1.5664$ bohr (below), in au. Truncated values of minimum ÷ maximum ÷ step: $-0.10 \div 0.10 \div 0.01$.

more shielded than that of prismane, located in the boundary of the vortex, see Figure 5 in the present paper. The effect of the remote carbon atoms on the probe H nucleus virtually vanishes, due to cancelation of a spike-up and spike-down pair from furthest and closest portions of the small-radius diamagnetic vortex about each C nucleus.

The contribution of σ-ring currents on the triangular face to σ_{zz}^{H} can be rated via the three-dimensional perspective on top of Figure 7. Two disjoint low ridges of Σ_{zz}^{H}, corresponding to the smallest value, 0.01 au, in the contour map, are observed. One of them is raised on a path through two distant C nuclei, the other through the projection of the H probe on the triangular face, marked by a cross on the right of the map. The truncated maximum in the map on the bottom of the same figure is orders of magnitude bigger, proving that local effects dominate. A quantitative estimate of the contribution of the peripheral σ-ring currents on σ_{zz}^{H} was obtained integrating eq 3 in the region where the σ diatropic flow is more intense, between the planes at distance $z \pm 0.1$ bohr from the triangular face. The contribution is 0.612 ppm, that is, less than 2% of the total value 34.6. Allowing for these results, the contribution of delocalized σ-ring currents to σ_{zz}^{H} would seem comparatively negligible.

An attempt at interpreting magnetotropism of prismane via the average shielding[13] at the cage center would lead us seriously astray for two reasons:

(i) The nearly vanishing $\sigma_{av}^{CM} = (\sigma_{xx}^{CM} + \sigma_{yy}^{CM} + \sigma_{zz}^{CM})/3 \approx 1.3$ ppm is obtained by averaging big diagonal components with different sign, $\sigma_{xx}^{CM} = \sigma_{yy}^{CM} = -25.6$ ppm and $\sigma_{zz}^{CM} = 55.2$ ppm. Thus σ_{av}^{CM} is unsuitable for an assessment of magnetotropicity. Our RCM indicates that virtual cancelation of the average magnetic field induced at the cage center is due to the conflict of opposite paratropic and diatropic regimes at right angles to the rectangular and triangular faces, respectively.

(ii) The big negative σ_{xx}^{CM} is mostly determined by the intense paratropic circulation about the x axis. In fact, the shielding density $\Sigma_{xx}^{CM}(\mathbf{r})$ diverges to $-\infty$ in the vicinity of the origin: the deep central well is represented by a white area in the maps of Figure 9. However, the deshielding domain encompasses a wide neighborhood of CM, including not only the paramagnetic whirlpool around it, but also the closest portion of two diamagnetic vortices flowing about opposite C−C bonds. Contributions of different sign to σ_{xx}^{CM} arise from the opposite senses of closest and furthest portions of these vortices (the shielding density function changes sign on a boundary nodal line through their centers). The effect of an element of current depends on the inverse cube of the distance, therefore cancellation of contributions from near-by and remote parts of any closed circuit is incomplete. The former prevails. Therefore, σ_{xx}^{CM} is a spurious quantifier of paratropicity, as it is biased also by the inner portion of diamagnetic vortices about the C−C bonds.

Analogous conclusions are arrived at by analyzing the big negative σ_{xx} values of central shielding on the planes of four C and of four H nuclei, −59.5 and −54.6 ppm, respectively, see Table 3. The corresponding σ_{zz} are as big as 57.1 and 41.0 ppm, but the σ_{yy} components are much smaller, 8.7 and 4.4 ppm. No

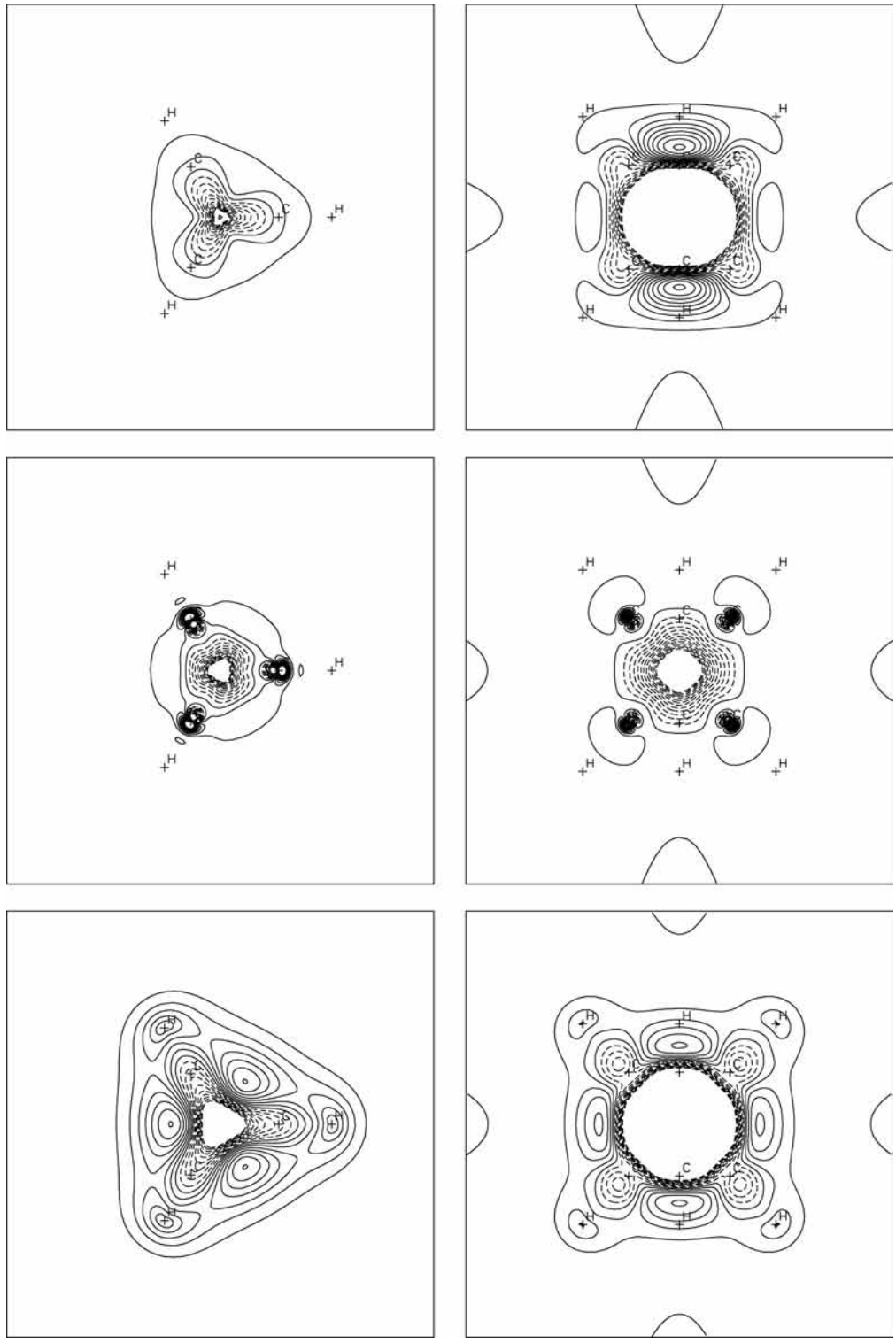

Figure 9. Magnetic shielding densities at cage and ring centers, Σ_{zz} (on the left) and Σ_{xx} (on the right) on three plot planes, through CM, C, and H nuclei (from top to bottom), in au. Minimum ÷ maximum ÷ step: for CM, −0.10 ÷ 0.10 ÷ 0.01; for C, −0.2 ÷ 0.2 ÷ 0.02; for H, −0.02 ÷ 0.02 ÷ 0.002. The shielding density function diverges for $\mathbf{r} \rightarrow 0$ and it is represented by a white area in a neighborhood of the central point.

plausible inference on magnetotropism of prismane could be made via the tiny σ_{av} reported in Table 3, that is, 2.1 and −3.1 ppm. Moreover, the deshielding domain of σ_{xx} shown in Figure 9 embraces an area much wider than the central paramagnetic vortex in Figures 4 and 5, because, also in these cases, negative contributions arise from that part of diamagnetic loops about C−C bonds and H nuclei nearest to the center.

Quite noticeably, the electron flow induced by a perpendicular magnetic field, strongly paramagnetic in the interior of the rectangular face, is diatropic all over the external region beyond the diamagnetic C−C vortices. The diatropic ring current regime is qualitatively similar to that induced by applying **B** normal to the triangular face, even if the intensity (0.06 au) is approximately half as large at the same distance from a C−C bond.

These findings are quite important, as they prove that inferring current regime on an open cell from magnitude and sign of the out-of-plane component of the shielding at its center may be

misleading. Taking into account σ_{av}^{CM} for modeling magnetic response would take us further afield. Just the other way round, one should first of all construct a spatial model of electron flow whereby each component of tensor magnetic properties can separately be rationalized. The fundamental instruments to do the job are just stagnation graph and current density maps.

6. Concluding Remarks

The present paper is part of a series[26–30] showing that molecular magnetic properties can be rationalized via the Ampère and Biot−Savart relationships of classical electromagnetic theory, allowing for a magnetically induced electron current density vector field $\mathbf{J^B}(\mathbf{r})$ determined by quantum mechanical methods.

From a local point of view, all the interesting behavior of this field occurs around its zeroes, that is, the stagnation points at which the modulus $|\mathbf{J^B}(\mathbf{r})|$ vanishes. In the vicinity of these points the direction of $\mathbf{J^B}$ may radically change, giving rise to a vortex or a saddle, it may spiral inward or outward, or it may form a more complicated pattern. Values of magnetic tensor components are strongly affected by the features of the current density field. Therefore, a stagnation graph showing the set of points of vanishing $|\mathbf{J^B}(\mathbf{r})|$ provides a fundamental instrument for understanding magnetic response.

Maps of streamlines and moduli of the $\mathbf{J^B}$ field and of the Jameson−Buckingham shielding density[22,23] constitute a complementary toolkit, which was used in the present study to develop a spatial ring current model of prismane and to interpret its magnetic susceptibility and nuclear magnetic shieldings.

The computer model constructed via Figures 1–5 shows that an external magnetic field applied perpendicularly to either a triangular or rectangular prism face induces paratropic electron currents about the center. The paramagnetic vortex around the C_3 symmetry axis is very weak. Its contributions to magnetic susceptibility and to magnetic shielding of C and H nuclei are expected to be negligible. On the other hand, the paratropic currents that flow about a C_2 axis are very strong all over a wide domain, covering a large part of a rectangular face and extending in the vertical direction.

Remarkably enough, a delocalized diatropic ring current flows in the external regions beyond the carbon skeleton of both faces, even if its intensity at the same distance from a C−C bond is two times stronger on the plane of a C-triangle. On the rectangular face, its modulus is 0.06 au, comparable with benzene π -ring current computed at the same level of theory, 0.08 au in the 1 a_0 plane.

Therefore, the peculiar magnetic properties of prismane depend on a mix of competing regimes in different directions: diatropism (paratropism) is observed at right angles to a triangular (rectangular) face. This determines enhanced anisotropy of magnetic susceptibility, $\Delta\chi \approx -80 \times 10^{-29}$ JT^{-2}. Both diamagnetic and paramagnetic contributions to the $\chi_\perp$ component are, in absolute value, much bigger than $\chi_{||}$ ($\perp$ and $||$ correspond to directions of C_2 and C_3 symmetry axes, normal to the rectangular and triangular faces, respectively) On the other hand, the strong anisotropy of magnetic shielding at carbon nuclei is due to an intense diamagnetic vortex that causes upfield shift of the σ_{zz}^{C} component. This local vortex enhances also the σ_{zz}^{H} component, which does not appear to be significantly biased by delocalized diatropic σ-ring currents. Proton shielding density maps show that their contributions to σ_{zz}^{H} are comparatively negligible.

Acknowledgment. Support from the Italian MURST via PRIN funds is gratefully acknowledged.

Supporting Information Available: Magnetizability and nuclear magnetic shielding values; magnification of the figure maps. This material is available free of charge via the Internet at http://pubs.acs.org.

References and Notes

(1) Lemalz, D. M.; Lokensgard, J. P. *J. Am. Chem. Soc.* **1973**, *88*, 5934–5935.
(2) Katz, T. J.; Acton, N. *J. Am. Chem. Soc.* **1973**, *95*, 2738–2739.
(3) Ladenburg, A. *Chem. Ber.* **1869**, *2*, 140–142.
(4) Kekulé, A. *Chem. Ber.* **1869**, *2*, 362–365.
(5) Randić, M.; Majerski, Z. *J. Chem. Soc. B* **1968**, 1289–1291.
(6) Teijiro Yonezawa, K. S.; Kato, H. *Bull. Chem. Soc. Jpn.* **1968**, *41*, 2336–2342.
(7) Woodward, R. B.; Hoffmann, R. *Angew. Chem., Int. Ed. Engl.* **1969**, *8*, 781–853.
(8) Baird, N. C.; Dewar, M. J. S. *J. Am. Chem. Soc.* **1969**, *91*, 352–355.
(9) Li, Z.; Rogers, D. W.; McLafferty, F. J.; Mandziuk, M.; Podosenin, A. V. *J. Phys. Chem. A* **1999**, *103*, 426–430.
(10) Priyakumar, U. D.; Dinadayalane, T. C.; Sastry, G. N. *New J. Chem.* **2002**, *26*, 347–353.
(11) Politzer, P.; Seminario, J. M. *Struct. Chem.* **1990**, *1*, 29–32.
(12) Gough, K. M.; Dwyer, J. R.; Dawes, R. *Can. J. Chem.* **2000**, *78*, 1035–1043.
(13) Moran, D.; Manoharan, M.; Heine, T.; von Ragué Schleyer, P. *Org. Lett.* **2003**, *5*, 23–26.
(14) Lazzeretti, P. Electric and Magnetic Properties of Molecules In *Handbook of Molecular Physics and Quantum Chemistry*; John Wiley & Sons, Ltd.: Chichester, U.K., 2003; Vol. 3, Part 1, Chapter 3.
(15) Hirschfelder, J. O. *J. Chem. Phys.* **1978**, *68*, 5151–5162.
(16) McWeeny, R. *Phys. Rev.* **1962**, *126*, 1028–1034.
(17) McWeeny, R. *Quantum Mechanics: Methods and Basic Applications*; Pergamon Press: Oxford, U.K., 1969.
(18) McWeeny, R. *Methods of Molecular Quantum Mechanics*; Academic Press: London, 1989.
(19) Jackson, J. D. *Classical Electrodynamics*, 3rd ed.; John Wiley & Sons: New York, 1999 p. 178.
(20) Lazzeretti, P.; Malagoli, M.; Zanasi, R. *Chem. Phys. Lett.* **1994**, *220*, 299–304.
(21) Lazzeretti, P. Ring Currents In *Progress in Nuclear Magnetic Resonance*; Emsley, J. W., Feeney, J.,. Sutcliffe, L. H., Eds.; Elsevier: New York, 2000; Vol. 36.
(22) Jameson, C. J.; Buckingham, A. D. *J. Phys. Chem.* **1979**, *83*, 3366–3371.
(23) Jameson, C. J.; Buckingham, A. D. *J. Chem. Phys.* **1980**, *73*, 5684–5692.
(24) Coddington, E. A.; Levinson, N. *Theory of Ordinary Differential Equations*; Mc Graw-Hill: New York, 1955.
(25) Gomes, J. A. N. F. *Phys. Rev. A* **1983**, *28*, 559–566.
(26) Pelloni, S.; Faglioni, F.; Zanasi, R.; Lazzeretti, P. *Phys. Rev. A* **2006**, *74*, 012506.
(27) Pelloni, S.; Lazzeretti, P.; Zanasi, R. *J. Phys. Chem. A* **2007**, *111*, 8163–8169.
(28) Pelloni, S.; Lazzeretti, P.; Zanasi, R. *J. Phys. Chem. A* **2007**, *111*, 3110–3123.
(29) Pelloni, S.; Lazzeretti, P. *Theor. Chem. Acc.* **2007**, *117*, 903–913.
(30) Pelloni, S.; Lazzeretti, P. *Theor. Chem. Acc.* **2007**, *118*, 89–97.
(31) Zanasi, R.; Lazzeretti, P.; Malagoli, M.; Piccinini, F. *J. Chem. Phys.* **1995**, *102*, 7150–7157.
(32) Ferraro, M. B.; Faglioni, F.; Ligabue, A.; Pelloni, S.; Lazzeretti, P. *Magn. Reson. Chem.* **2005**, *43*, 316–320.
(33) Frisch, M. J.; Trucks, G. W.; Schlegel, H. B.; Scuseria, G. E.; Robb, M. A.; Cheeseman, J. R.; Zakrzewski, V. G.; Montgomery, J. A., Jr.; Stratmann, R. E.; Burant, J. C.; Dapprich, S.; Millam, J. M.; Daniels, A. D.; Kudin, K. N.; Strain, M. C.; Farkas, O.; Tomasi, J.; Barone, V.; Cossi, M.; Cammi, R.; Mennucci, B.; Pomelli, C.; Adamo, C.; Clifford, S.; Ochterski, J.; Petersson, G. A.; Ayala, P. Y.; Cui, Q.; Morokuma, K.; Malick, D. K.; Rabuck, A. D.; Raghavachari, K.; Foresman, J. B.; Cioslowski, J.; Ortiz, J. V.; Stefanov, B. B.; Liu, G.; Liashenko, A.; Piskorz, P.; Komaromi, I.; Gomperts, R.; Martin, R. L.; Fox, D. J.; Keith, T.; Al-Laham, M. A.; Peng, C. Y.; Nanayakkara, A.; Gonzalez, C.; Challacombe, M.; Gill, P. M. W.; Johnson, B. G.; Chen, W.; Wong, M. W.; Andres, J. L.; Head-Gordon, M.; Replogle, E. S.; Pople, J. A. *Gaussian 98*, revision A.7; Gaussian, Inc.: Pittsburgh, PA, 1998.
(34) Lazzeretti, P.; Malagoli, M.; Zanasi, R. Technical Report on Project " Sistemi Informatici e Calcolo Parallelo", Research Report 1/67, CNR, 1991.
(35) Zanasi, R. *J. Chem. Phys.* **1996**, *105*, 1460–1469.
(36) Woon, D. E.; Dunning, T. H., Jr *J. Chem. Phys.* **1993**, *98*, 1358–1371.

(37) The LINUX and WINDOWS versions of the graphic code used to obtain three-dimensional representations of the stagnation graph and current density vector field of a series of molecules can be downloaded at https://theochem.chimfar.unimo.it/VEDO3/.

(38) Gomes, J. A. N. F. *J. Chem. Phys.* **1983**, *78*, 4585–4591.

(39) Milnor, J. W. *Topology from the Differentiable Viewpoint*; University of Virginia Press: Charlottesville, VA, 1997.

(40) Guillemin, V.; Pollack, A. *Differential Topology*; Prentice-Hall: Englewood Cliffs, 1974.

(41) Pelloni, S.; Ligabue, A.; Lazzeretti, P. *Org. Lett.* **2004**, *6*, 4451–4454.

(42) Soncini, A.; Fowler, P. W.; Lazzeretti, P.; Zanasi, R. *Chem. Phys. Lett.* **2005**, *401*, 164–169.

JP711996N